ADVANCED SUSTAINABLE SYSTEMS
www.advsustainsys.com

Polymerized Riboflavin and Anthraquinone Derivatives for Oxygen Reduction Reaction

Nadine Kleinbruckner, Elisabeth Leeb, Dominik Wielend, Corina Schimanofsky, Munise Cobet, Felix Mayr, Angelina Kerschbaumer, Cigdem Yumusak, Jan Richtar, Markus Clark Scharber, Helmut Neugebauer, Mihai Irimia-Vladu, Jozef Krajcovic, and Niyazi Serdar Sariciftci*

Hydrogen peroxide (H_2O_2) is identified as a promising reagent for fuel cells, reducing the dependency on carbon-based fuels. In this work, electrochemically synthesized polymers are employed to improve the efficiency of the oxygen (O_2) reduction reaction, thus producing H_2O_2 in an environmentally friendly way. Two aminoanthraquinones, as well as riboflavin (vitamin B2), are successfully immobilized via oxidative electropolymerization onto both glassy carbon and carbon paper. Of the investigated compounds, polyriboflavin shows a high Faradaic efficiency toward O_2 reduction, even at a very low potential of only −0.1 V versus SHE. This catalytic effect is present in neutral and alkaline conditions, using both glassy carbon and carbon paper, but highly pronounced in neutral, aqueous solutions.

1. Introduction

In recent decades, much effort has been put into developing reliable energy storage systems for renewable energy sources such as wind or solar energy.[1–3] Even though conventional energy storage systems such as batteries and electrolyzers mainly employ inorganic materials, organic materials have steadily gained attention in the scientific community as an environmentally friendly alternative.[4–10] Synthetic fuels have been presented as a promising technology to enable the full potential of renewable energy sources. Such chemicals can be easily transported and employed without a complete change of our energy vectors and their distribution networks. These synthetic fuels can be regarded as storing renewable electrical energy in chemical bonds.[11–14] If they can replace fossil fuels on a large scale, the net carbon dioxide emission to the atmosphere could be curbed.

Aside from carbon-based fuels, hydrogen peroxide (H_2O_2) has been identified as a promising candidate as a synthetic fuel for chemical energy storage.[15] Its only decomposition products are oxygen (O_2) and water (H_2O). Furthermore, it is a stable liquid that can easily be transported and stored.[16–19] H_2O_2 is mainly produced via the anthraquinone process on an industrial scale, which involves organic solvents and extensive purification steps.[17,18] Thus, alternative routes of production have been explored. The oxygen reduction reaction (ORR) is an energy-efficient and environmentally friendly production pathway of H_2O_2. It involves the 2 e^- reduction process of O_2, which is, however, competing with the 4 e^- reduction pathway, producing water.[20] The ORR can be performed in aqueous solutions under ambient pressure, bypassing the need for organic solvents. Both noble metal catalysts, such as Au nanostructures[21–23] or carbon-coated metal nanoparticles,[24,25] and non-noble metal catalysts, such as porous carbon structures,[26,27] doped carbon,[28–31] organic conjugated systems,[32,33] conducting polymers[34–36] or metal–organic complexes[37,38] have been identified as suitable catalytic systems for the 2 e^- reduction pathway to H_2O_2.

Quinones have been used in multiple modifications for electrocatalysis.[39,40] Anthraquinones especially have been employed for both ORR[41–44] as well as electrochemical carbon dioxide capture.[45–49] The catalytic activity of flavin derivatives has been studied in both homogeneous[50–52] and heterogeneous[53–57] systems. The tendency of both synthetic as well as naturally occurring flavines toward oxygen reduction has been investigated by numerous groups.[58,59] Recently we have reported the Faradaic efficiency of the naturally occurring riboflavin (RF), also known as vitamin B2, concerning the ORR in homogeneous solution.[44,60] Herein we found a strong

N. Kleinbruckner, E. Leeb, D. Wielend, C. Schimanofsky, M. Cobet, F. Mayr, A. Kerschbaumer, C. Yumusak, M. C. Scharber, H. Neugebauer, M. Irimia-Vladu, N. S. Sariciftci
Linz Institute for Organic Solar Cells (LIOS)
Institute of Physical Chemistry
Johannes Kepler University Linz
Altenberger Straße 69, Linz 4040, Austria
E-mail: elisabeth.leeb@jku.at

J. Richtar, J. Krajcovic
Faculty of Chemistry
Materials Research Centre
Brno University of Technology
Purkynova 118, Brno 612 000, Czech Republic

The ORCID identification number(s) for the author(s) of this article can be found under https://doi.org/10.1002/adsu.202300352

DOI: 10.1002/adsu.202300352

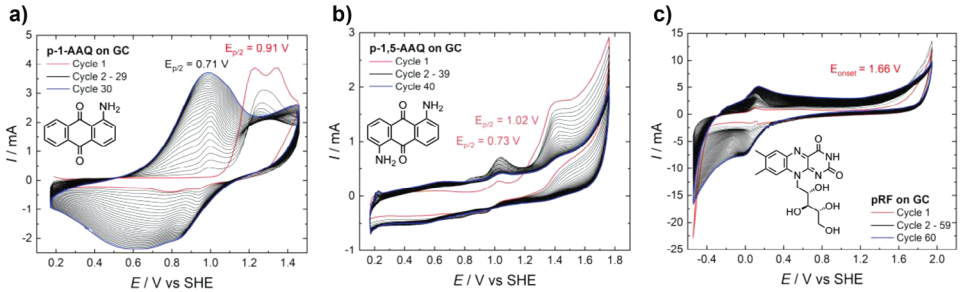

Figure 1. CVs of electropolymerization of a) p-1-AAQ and b) p-1,5-AAQ in 6 M H_2SO_4 and c) pRF in 0.1 M H_2SO_4 on GC with the chemical structure of the respective monomer. The first cycle (red) and the last cycle (blue) are indicated.

dependence on both pH and electrode material, with higher productivity achieved under alkaline conditions.

Homogeneous catalytic systems suffer from poor stability and elaborate catalyst recovery.[61,62] Moreover, most catalysts, both organic and non-organic, offer only limited solubility, thus further impeding their efficiency.[61] Immobilizing the catalyst on the surface of the electrode improves longevity while simultaneously simplifying the recovery of the product.[40,63] Additionally, the immobilization of the catalyst may facilitate the transfer of electrons from the electrode to the catalyst.[64]

This work aims to demonstrate the electropolymerization of the three electrocatalysts 1-aminoanthraquinone (1-AAQ), 1,5-diaminoanthraquinone (1,5-AAQ), and riboflavin (RF). Two different carbon-based electrode materials, glassy carbon, and carbon paper, were chosen as substrates displaying different surface areas and properties, which were studied in aqueous media at various pH values. The catalytic activity of the electrodes towards oxygen reduction was studied via H_2O_2 detection and Faradaic efficiency (FE) calculation.

2. Results and Discussion

The CVs of the oxidative electropolymerization of the three polymers are depicted in **Figure 1**, with the first and last cycles marked. As shown in Figure 1a, the polymerization of 1-AAQ first shows an anodic peak at $E_{p/2}$ of 0.91 V, with the peak current decreasing throughout the first 10 cycles. This peak indicates oxidation of the amino group to a radical cation ($NH_2^{\cdot+}$) and the corresponding dication (NH_2^{2+}),[65–68] followed by a rapid reaction of the charged species forming oligomers. Thus, only a small reductive peak can be observed, as most ionic species have reacted previously. Furthermore, a reversible redox peak is growing after the first cycles at an $E_{p/2}$ of 0.71 V, which is due to the formation of the conductive polymer.[69]

The electropolymerization of 1,5-AAQ depicted in Figure 1b follows a similar trend to the polymerization of 1-AAQ, with an anodic peak at $E_{p/2}$ of 0.73 V and a second redox peak at 1.02 V, resulting from the oxidation of the monomer to a radical cation and dication. To ensure the sufficient formation of cations, the oxidative vertex potential had to be increased compared to 1-AAQ to a more anodic potential, as was reported previously.[68]

Similar to the previously discussed examples, the electropolymerization of RF depicted in Figure 1c shows a large oxidative peak at an onset potential of 1.66 V. Interestingly, the current increases during the second cycle as radicals are formed and then decreases again as the radicals combine while forming the polymeric chain. This decrease in anodic peak current reverts after ≈10 cycles as a conducting film is formed on top of the electrode. Furthermore, for the first cycles, the characteristic reduction feature of polyriboflavin below 0.2 V is very pronounced and separated, becoming less defined with additional cycles as the polymer is formed. In contrast to reports found in literature,[70] polymerization in sulfuric acidic solutions yielded the most favorable results in our case. A clear film formation could be seen on top of the glassy carbon electrode with a significant increase of the characteristic redox peaks of RF seen in the CV. The polymerization of RF in pH 7 and 13, which can be found in Figure S2 (Supporting Information), showed a minor current increase with no visible film formation.

All polymers have also been polymerized onto carbon paper electrodes. The CVs for those polymerizations, found in Figure S3 (Supporting Information), show similar trends with sharper features compared to glassy carbon due to the difference in the surface of the two electrode materials.

In **Figure 2**, SEM images of p-1-AAQ, p-1,5-AAQ, and pRF on carbon paper can be seen.

As shown in Figure 2b, p-1-AAQ has a sponge-like appearance, partially coating the carbon paper strands, which has a similar texture to that of pANI.[34] A similar appearance can be seen on a glassy carbon electrode depicted in Figure S4 (Supporting Information). In contrast, p-1,5-AAQ and pRF appear to form a much thinner, less pronounced film that can be seen on top of the carbon paper. When comparing the images with bare, uncoated carbon paper, as shown in Figure 2a, a knob-like coating can be seen on the carbon fibers. On glassy carbon, both p-1,5-AAQ and pRF form a thin film on the electrode, which can be seen by the naked eye as a black film in the case of p-1,5-AAQ and a reflective, iridescent film in the case of pRF. After electrolysis, the film can be distinguished from the electrode in SEM images, as bubbles form in the p-1,5-AAQ, and cracks and tendrils can be found on the pRF, depicted in **Figure 3**.

ATR-FTIR spectra of the monomer and polymers are depicted in **Figure 4**.

When comparing the IR spectra of the monomer and polymer of the AQ-based polymers depicted in Figure 4a,b, in both cases, the NH-stretching vibrations found at ≈3300 and 3420 cm^{-1} broaden and disappear upon the polymerization, which is in accordance with literature.[68,71] The polymerization occurs via NH-linkers. Additionally, the polymeric spectra display much broader, less defined peaks than the monomers, further

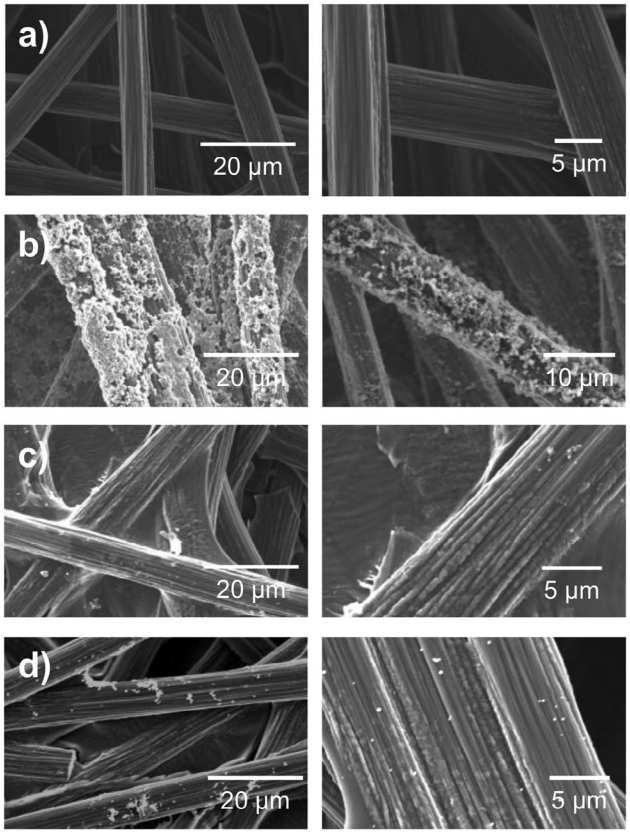

Figure 2. SEM images of a) uncoated CP as well as b) p-1-AAQ, c) p-1,5-AAQ, and d) pRF on CP.

indicating a successful polymerization. This behavior is especially noticeable in Figure 4b, where the bands at 1605 and 1542 cm^{-1} broaden significantly.[68,72] Since p-1-AAQ possesses the same backbone as the already well-studied polymer pANI, the IR spectrum of pANI was studied as well and can be found in Figure 4c, with the polymerization depicted in Figure S5 (Supporting Information). As can be seen, upon polymerization pANI shows the same peak broadening at 1567 and 1485 cm^{-1}, while the NH-stretching vibrations at 3431 and 3350 cm^{-1}

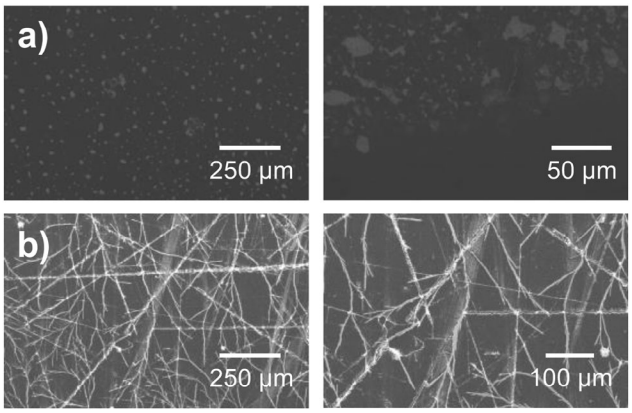

Figure 3. SEM images of a) p-1,5-AAQ and b) pRF on GC after electrolysis.

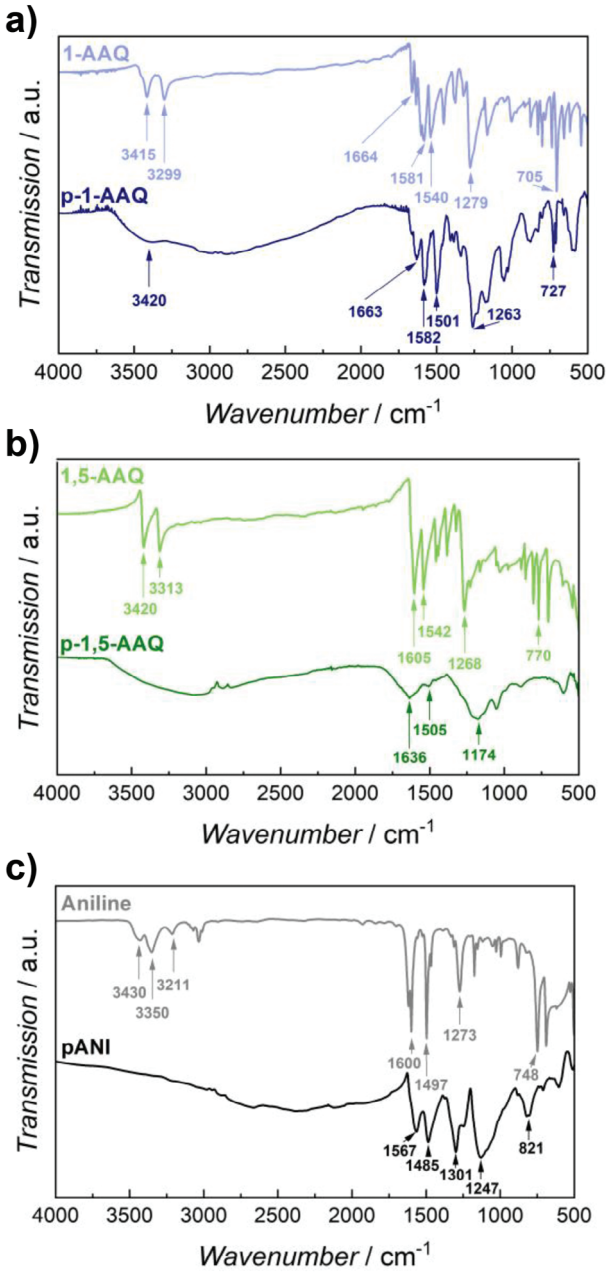

Figure 4. IR spectra of monomer and polymer for a) p-1-AAQ, b) p-1,5-AAQ, and c) pANI.

disappear.[73–75] A table on the complete assignment of the IR spectra can be found in Table S1 (Supporting Information). Furthermore, the Raman spectra of 1-AAQ and p-1-AAQ can be found in Figure S6 (Supporting Information). The bathochromic shift of the carbonyl stretching vibration at 1658 and 1644 cm^{-1} is in accordance with literature reports.[76–78]

Due to the broad electrochemical range required for the polymerization of pRF, no polymerization on a non-carbon-based electrode was achieved, and thus no IR spectra were measured. However, both the CV as well as the visible film formation, further supported by SEM images, provide suitable proof for the

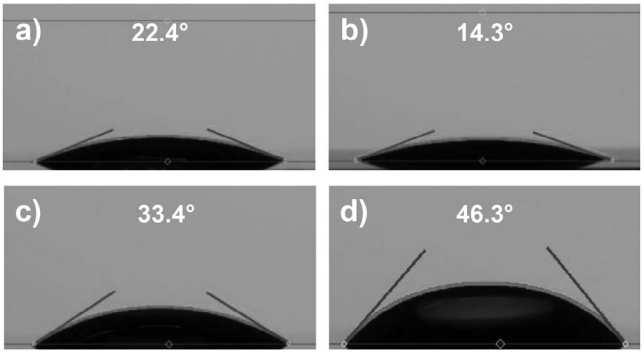

Figure 5. Contact angle measurement using 18 MΩ water on a) bare GC, b) p-1-AAQ, c) p-1,5-AAQ, and d) pRF.

successful polymerization – in addition to literature reports. The XPS spectra of the three investigated polymers are shown in Figure S7 (Supporting Information). The N1s spectra of p-1-AAQ and p-1,5-AAQ show signatures of substituted aromatic amine moieties (399.4 and 399.3 eV, respectively), aromatic -NH_2 groups (401.0 and 400.5 eV, respectively) as well as protonated/positively charged amine groups at higher binding energies. Compared to p-1-AAQ and p-1,5-AAQ, pRF shows N1s XPS peaks at a lower binding energy of 398.4 eV, which may be attributed to the imine moieties in the aromatic rings. In addition to this peak, the material displays peaks attributed to the substituted aromatic amine and amide moieties (400.0 eV) and positively charged nitrogen atoms (401.4 eV).

Additionally, EIS measurements have been used to determine the conductivity of the polymer samples on glassy carbon. The results and the equivalent circuit used to fit the data can be seen in Figure S8 (Supporting Information). The equivalent circuit for the fitting was chosen from the literature of Gasiorowski et al.[79] due to the similarity of the investigated samples. Thus, resistance values for R_2 were used to characterize the polymeric layer on top of the electrode. The conductivity could be calculated using the film thicknesses of 1600 nm for p-1-AAQ, 65 nm for p-1,5-AAQ, and 150 nm for pRF. This difference in film thicknesses between the polymers is also clearly visible in the SEM images displayed in Figure 2, where p-1-AAQ appears to be quite spongy and porous compared to the thin films of p-1,5-AAQ and pRF. The lowest conductivity was found for p-1,5-AAQ, with values $\approx 10^{-9}$ S cm^{-1}. pRF displays a slightly higher conductivity of $\approx 5 \times 10^{-9}$ S cm^{-1} and the highest values were reached for p-1-AAQ at 2×10^{-8} S cm^{-1}. These values are in the range of undoped pANI.[80,81]

Contact angle measurements were performed to further characterize the aqueous wetting behavior of the polymeric film on top of the electrode. The results of the measurements on glassy carbon electrodes can be found in **Figure 5**. As shown in Figure 5a, bare glassy carbon is highly hydrophilic with a contact angle of 22.4°, which is due to the electrochemical activation procedure. The contact angle measurement for bare, untreated glassy carbon can be found in Figure S9 (Supporting Information) and displays a contact angle at a mean value of 75.5°, which is in accordance with literature values.[82] Interestingly, p-1-AAQ exhibits high hydrophilicity at 14.3°, lowering the wettability of the glassy carbon electrode. Furthermore, p-1,5-AAQ has a lower hydrophilicity than its counterpart p-1-AAQ, at a contact angle of

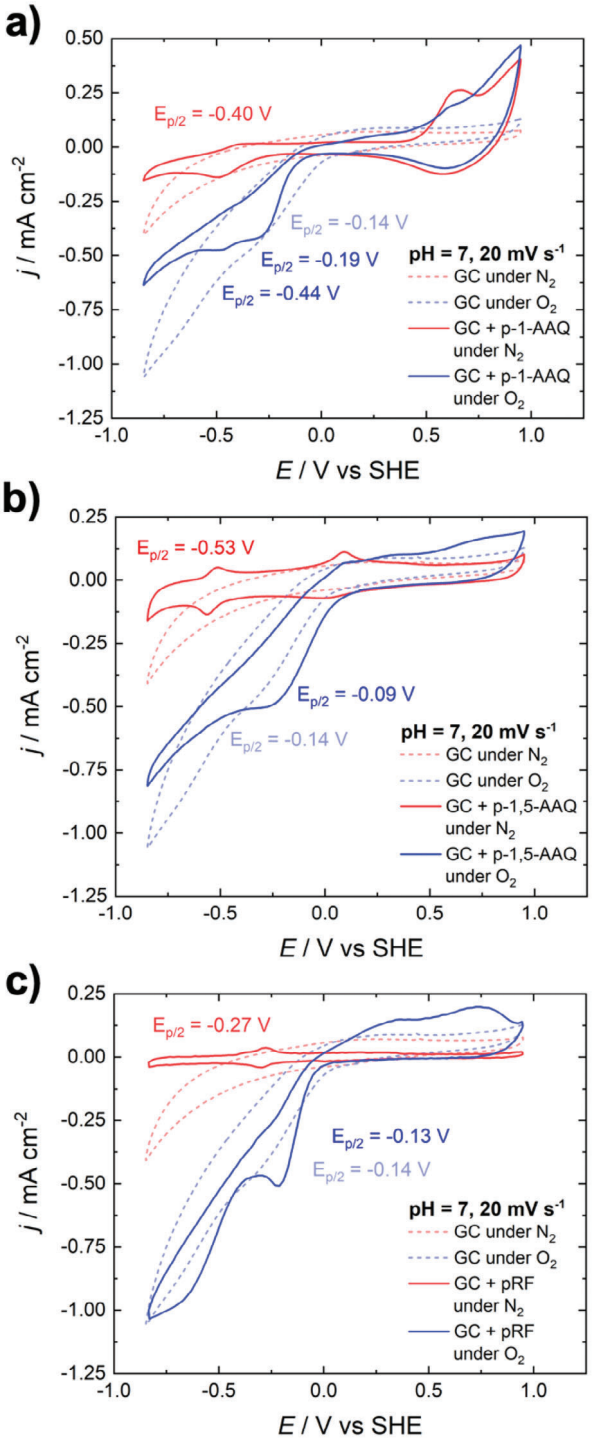

Figure 6. CVs of a) p-1-AAQ, b) p-1,5-AAQ, and c) pRF in pH 7 on a GC electrode at 20 mV s^{-1}.

33.4°. pRF displays the lowest hydrophilicity at an angle of 46.3°, which is, however, still less hydrophobic than bare glassy carbon without any activation.

The electrochemical activity towards the ORR was studied for all materials. The CVs of the polymer-coated glassy carbon electrodes under neutral conditions can be found in **Figure 6**. As

Table 1. Moles of H_2O_2 produced and faraday efficiency (FE) of the chronoamperometric measurements at −0.1 V using the polymer-coated GC and CP electrodes as well as reference measurements using uncoated electrodes.

pH value	without polymer		p-1-AAQ		p-1,5-AAQ		pRF	
	n / µmol	*FE* / %	*n* / µmol	*FE* / %	*n* / µmol	*FE* / %	*n* / µmol	*FE* / %
Glassy Carbon								
pH 7	12.6	57	5.7	72	21.7	61	26.0	90
pH 12	0.8	2	9.0	68	10.8	65	9.5	94
Carbon Paper								
pH 7	0.4	16	16.2	55	6.4	18	70.1	85
pH 12	0.6	20	0.3	1	0.4	1	29.0	62

can be seen from Figure 6a, the oxygen reduction on a p-1-AAQ modified glassy carbon electrode is shifted to a slightly more cathodic potential at a decreased current density. The reduction of p-1-AAQ itself, which is visible under N_2 saturated conditions, also slightly shifts in potential upon the presence of oxygen. In contrast, p-1,5-AAQ found in Figure 6b slightly anodically shifts the reduction of oxygen. Among the three different polymers investigated in this work, pRF is the only one that both boosts the current density of the oxygen reduction compared to untreated glassy carbon while in parallel also shifting the onset of the reduction to a more anodic potential, as seen in Figure 6c. A similar trend is found under acidic and alkaline conditions, where pRF is the only polymer increasing the current density and thus facilitating oxygen reduction. The CVs at pH 2 and 12 can be found in Figure S10 (Supporting Information).

To determine the influence of the electrode material on the electrochemical oxygen reduction, the CVs of polymer-coated carbon paper electrodes in the neutral phosphate buffer can be found in **Figure 7**. Upon the use of carbon paper as electrode material instead of glassy carbon, all polymers anodically shift the onset of the ORR. Even though this shift facilitates the reduction of oxygen, a higher current density is reached when using bare carbon paper, especially at cathodic potentials, which is also the case under acidic and alkaline conditions depicted in Figure S11 (Supporting Information).

The cyclic stability of the polymers was investigated at a scan rate of 20 mV s^{-1} for 100 cycles under O_2. The results can be found in Figure S12 (Supporting Information), where p-1,5-AAQ and pRF display remarkable cyclic stability, losing less than 25% of the initial peak current density. In contrast, p-1-AAQ displays more rapid degradation, especially on carbon paper, where, after 100 cycles, less than 45% of the initial current density can still be detected in the CV. The morphology of the glassy carbon electrodes was studied after repeated cycling, with the SEM images depicted in Figure S13 (Supporting Information). As shown in Figure S13a (Supporting Information), p-1-AAQ does not show any visible degradation, as the morphology of the polymer appears to be unchanged above and below the electrolyte line visible in the image. In comparison, p-1,5-AAQ and pRF both show the same degradation after repeated cycling as after chronoamperometric measurements depicted in Figure 3.

To study the applicability of these polymers as electrocatalysts for the production of H_2O_2, chronoamperometric measurements have been performed over 6 h at a potential of −0.1 V, where catalytic effects from the polymers are observed from CV studies in Figure 6 and Figure 7. As this low potential is insufficient to facilitate oxygen reduction in acidic media, only neutral and alkaline electrolyte solutions were chosen. The results can be found in **Table 1**. The corresponding time versus current transient curves for all chronoamperometric measurements can be found in Figure S14 (Supporting Information). The detailed results over time of the chronoamperometry can be found in Figure S15 (Supporting Information) at pH 7 and Figure S16 (Supporting Information) at pH 12.

As seen in Table 1, at a constant potential of −0.1 V, the bare electrodes have a very low intrinsic activity, with a low productivity of below 15 µmol and a low selectivity for H_2O_2 at FEs below 65%. When using glassy carbon electrodes coated with p-1-AAQ or p-1,5-AAQ, a slight increase can be found in selectivity, as efficiencies rise above 60% under all conditions. However, the p-1-AAQ-coated glassy carbon electrode at pH 7 shows a lower productivity of 5.7 µmol H_2O_2 produced throughout 6 h while still increasing the efficiency. It seems p-1-AAQ acts as a peroxide directing layer rather than a true electrocatalyst similar to pANI in acidic media.[34] Here, p-1-AAQ prevents the ORR via the 4 e^- pathway, facilitating the reduction to H_2O_2 and thus raising the FE. However, no increase in production is found under these conditions, as active centers might be inhibited.

When using coated carbon paper electrodes, under neutral conditions efficiencies slightly increase to 55% for p-1-AAQ and 18% for p-1,5-AAQ. This behavior is not found under alkaline conditions, as both p-1-AAQ and p-1,5-AAQ coated electrodes show less activity toward oxygen reduction than the intrinsic activity of the bare electrodes.

In contrast, pRF-coated electrodes improve both the selectivity and the productivity under all investigated conditions compared to bare electrodes. Especially noticeable is the improved productivity of H_2O_2 when using pRF, as the highest amount of 70.1 µmol over 6 h was reached when using a pRF-coated carbon paper electrode under neutral conditions. This value is especially remarkable due to the low potential used for these chronoamperometric measurements. The results of the pRF-coated electrodes can be found in **Figure 8**.

As can be seen, both the amount of H_2O_2 produced and the FE increased upon using pRF-coated electrodes compared to uncoated ones. This increase is independent of the electrode material and pH of the electrolyte. An astounding increase in FE can be seen when using a glassy carbon pRF-coated working electrode in alkaline conditions, as the mean efficiency increases

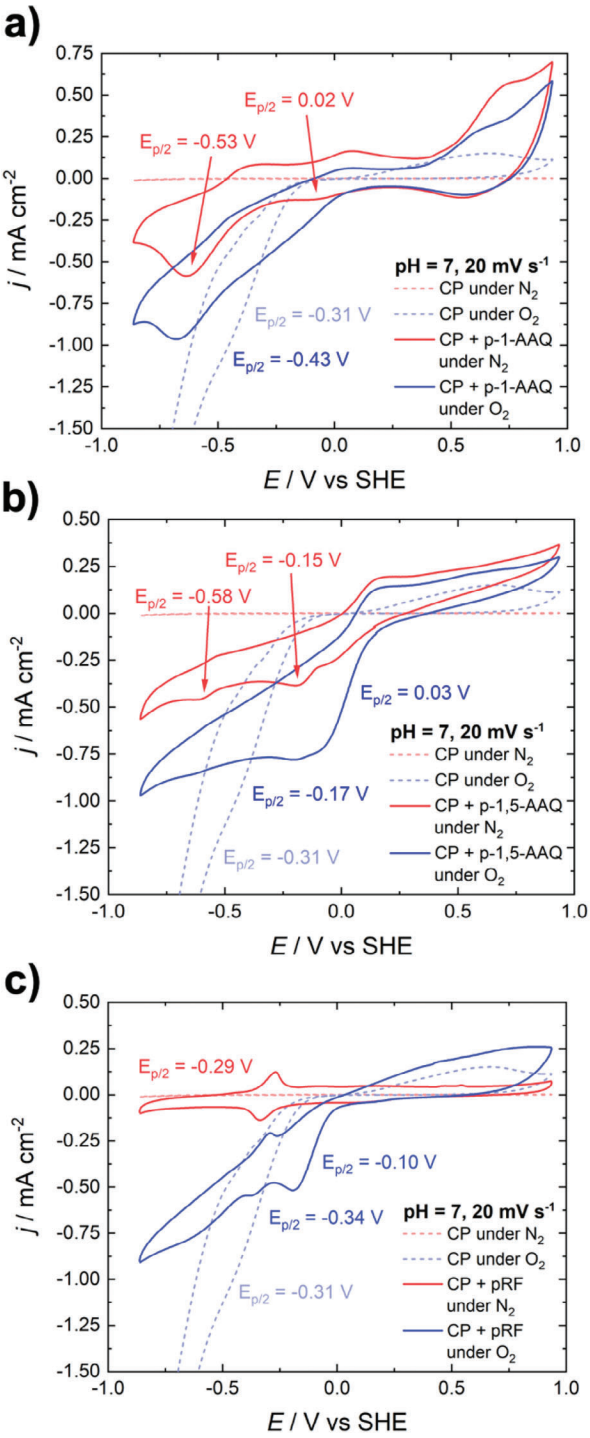

Figure 7. CVs of a) p-1-AAQ, b) p-1,5-AAQ, and c) pRF in pH 7 on a CP electrode at 20 mV s^{-1}.

from 2% to 94%. At the same time, the highest productivity is reached using a carbon paper pRF-coated electrode in neutral conditions at 70.1 µmol over the span of 6 h.

In order to ensure that this increase in activity toward the ORR is indeed due to the presence of the polymer and not due to an unintended activation procedure, a carbon paper electrode has been pretreated in the same way akin to the polymerization of RF. However, no monomer was added to the solution, with the procedure otherwise performed as usual. The result can be seen in Figure S17 (Supporting Information). Even though, due to this pretreatment, the FE increased to a mean value of 64%, the productivity of H_2O_2 only shows 8.4 µmol, compared to 70.1 µmol when using a pRF-coated carbon paper electrode. This result further confirms the potent electrocatalytic performance of pRF.

Furthermore, we investigated the stability of the materials by elongating the chronoamperometric measurements up to a total duration of 20 h. The results for the cumulative amount of H_2O_2 produced and the faradaic efficiency using a glassy carbon electrode for this 20 h electrolysis can be found in Figure S18 and Table S2 (Supporting Information). It can be seen that even after 20 h, pRF displays the highest productivity at a total of 18.4 µmol produced. Furthermore, during the first 14 h, pRF retains a remarkable mean faradaic efficiency of 93%, exceeding all other materials. This efficiency drops to a mean value of 54% after 14 h, which still exceeds all other systems, as a drop off in efficiency can even be seen for a blank glassy carbon electrode.

This outstanding performance of pRF as an electrocatalyst for ORR was achieved while applying a very low potential of only −100 mV. Even though p-1-AAQ and p-1,5-AAQ improve the ORR when using a glassy carbon electrode, this increase in productivity or selectivity is less compared to when pRF is used, apart from slightly higher productivity of p-1,5-AAQ under alkaline conditions. However, when using carbon paper, the polymerized anthraquinones seem to hinder the selectivity toward oxygen reduction, compared to blank uncoated electrodes. At more negative potentials of −250 mV, all three polymers increase the electrochemical production of H_2O_2 using a glassy carbon electrode, as seen in Figure S19 (Supporting Information). However, at this potential, no electrocatalytic effect can be seen concerning FE, as uncoated glassy carbon performs equally as well in neutral conditions and even better than p-1-AAQ and p-1,5-AAQ in alkaline conditions.

Our previous study compared the electrocatalytic performance of homogeneous anthraquinones and riboflavin toward ORR[44]. In homogeneous systems, we found hydroxy-substituted anthraquinones to outperform the electrocatalytic activity of riboflavin. The exceptional activity of 1,8-dihydroxyanthraquinone has been reported previously.[39] However, as demonstrated in this work, heterogeneous pRF is evidently a superior electrocatalyst to p-1-AAQ and p-1,5-AAQ, which differs from the results in the solution. Similarly structured electrocatalysts such as quinacridone and epindolidione offer similar efficiencies as pRF of 96%, however, these studies were performed in highly acidic media.[33,83] Further product quantification has been performed on perylene tetracarbonyl imide, which offers structural similarities to anthraquinones. Here, an efficiency of 70% was reached, which was rapidly degrading throughout the electrolysis.[84] Comparing these previous studies to our results, pRF seems to be a remarkably efficient as well as stable electrocatalyst for ORR.

Interestingly, while previous work on polymerized anthraquinones has found an increase in the catalytic activity toward oxygen reduction with higher hydrophilicity,[85] in this work, pRF displays the highest hydrophobicity at 46.3° while obtaining the highest productivity and selectivity in

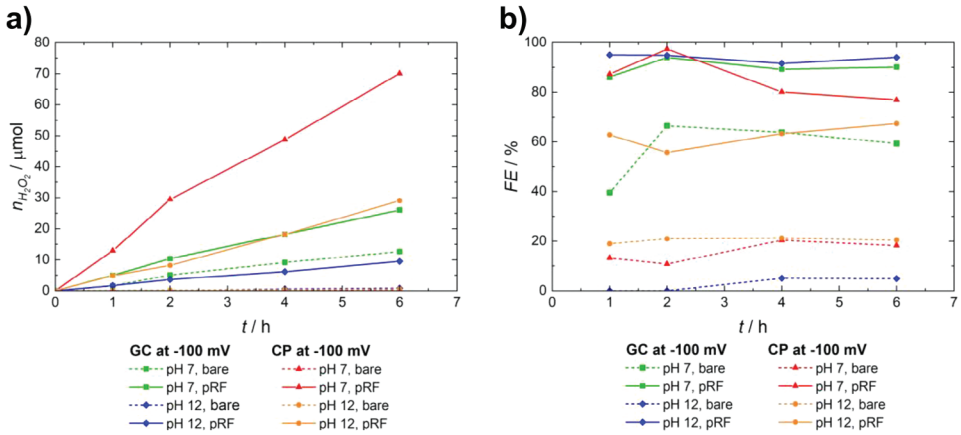

Figure 8. Results of chronoamperometric measurements at −100 mV using pRF on GC and CP with a) amount of H_2O_2 produced and b) FE for 6 h.

chronoamperometric experiments. These results seem to indicate an optimal wetting behavior of ≈45° to 50° to maximize the efficiency of ORR. Additional studies on the correlation between polymeric properties and efficient oxygen reduction are needed to understand these effects further in detail.

3. Conclusion

This work investigated electrochemically polymerized riboflavin and anthraquinone derivatives and their electrocatalytic ability toward oxygen reduction. The successful polymerization was validated using IR spectroscopy and SEM images. While p-1-AAQ formed sponge-like structures on top of the electrodes, similar to the already known electropolymerized pANI, p-1,5-AAQ and pRF formed a very thin and hardly observable film on top of the surface of both glassy carbon and carbon paper.

Electrochemical studies of the polymer-coated electrodes showed improved efficiency for pRF under both neutral and alkaline conditions. These efficiencies were obtained while employing a relatively low potential of −0.1 V, while reaching a maximum amount of 70.1 µmol of H_2O_2. Nevertheless, this amounts to an astounding eightfold increase in productivity compared to bare, uncoated electrodes.

4. Experimental Section

Electrochemical Polymerization: Prior to any polymerization, glassy carbon (GC) plate electrodes (1 × 4 cm, 2 mm, Alfa Aesar) were polished using Al_2O_3 pastes (Buehler Micropolish II deagglomerated) with particle sizes of 1.0, 0.3, and 0.05 µm. The electrodes were sonicated in 18 MΩ water and isopropanol between each polishing step. An activation procedure was performed before the electrodes were used, which consisted of sweeping the potential between 0.85 and 1.65 V at a scan rate of 50 mV s^{-1} for 30 cycles in an electrolyte solution of 0.5 M H_2SO_4.

Carbon paper (CP, TGP-H 60, Alfa Aesar) electrodes were cut to size and contacted using a copper wire. For spectroscopic analysis, Cr / Au-coated electrodes were prepared by cutting glass substrates to a size of 0.7 cm × 6 cm and thoroughly cleaning them with various organic solvents. The glass slides were treated in a plasma oven (Plasma ETCH P25 plasma, O_2, 2 min), after which 5 nm of Cr were evaporated with 1.5 A and a rate of 0.04 nm s^{-1}, followed by the evaporation of 100 nm of Au at ≈10^6 mbar.

The standard procedure for electrochemical polymerization of both anthraquinone derivatives was performed in 6 M H_2SO_4 using a saturated calomel electrode as a reference electrode and a platinum foil (Pt) as counter electrode. Both monomers were purified by train sublimation before being used. The polymerization of 1-aminoanthraquinone (1-AAQ, Alfa Aesar) was performed according to a procedure by Badawy et al.[65] A 5 mM solution of 1-AAQ was purged with N_2 for 30 min, after which the potential was swept from 0.16 to 1.46 V at a scan rate of 100 mV s^{-1} for 30 cycles to yield p-1-AAQ. To produce p-1,5-AAQ, the procedure was slightly modified by using a solution of 2.5 mM 1,5-AAQ (Alfa Aesar), increasing the oxidative vertex to 1.76 V and decreasing the scan rate to 50 mV s^{-1}. The polymerization of aniline (Sigma–Aldrich) was performed according to literature.[34,86–88]

The standard procedure of the oxidative electropolymerization of riboflavin (RF, Sigma–Aldrich) was based on a procedure by Ivanova et al.[89] and Radzevic et al.[70] and further optimized. A 1 mM solution of RF in 0.1 M H_2SO_4 was purged with N_2 for 30 min. A commercial Ag/AgCl (3 M KCl) reference electrode and a Pt foil counter electrode were used, and the potential was swept from −0.55 to 1.95 V for 60 cycles at a scan rate of 50 mV s^{-1}.

Standard procedures were used for all polymerizations if not otherwise indicated.

Electrochemical Experiments: If not indicated otherwise, all potentials throughout this work were recalculated and stated versus SHE.

Cyclic voltammetry (CV), as well as electrolysis experiments, were performed in a two-compartment cell separated by a Nafion membrane (117, Alfa Aesar). The respective, modified electrode was used as the working electrode (WE), while a Pt foil was used as the counter electrode (CE), and a commercial Ag/AgCl (3 M KCl) electrode (BASi) was used as the reference electrode (RE). Half-step potentials ($E_{p/2}$) were obtained by reading the potential of the CV at half of the peak signal current. For the electrolyte solutions, a 0.1 M phosphate buffer was prepared from H_3PO_4 (Sigma–Aldrich) and NaH_2PO_4 (Sigma–Aldrich) at pH 2, from NaH_2PO_4 and Na_2HPO_4 (Sigma–Aldrich) at pH 7 and from Na_2HPO_4 and Na_3PO_4 (Thermo Scientific) at pH 12. All electrochemical experiments were performed either on an IPS Jaissle Potentiostat / Galvanostat PGU 10 V – 100 mA or a Jaissle Potentiostat / Galvanostat 1030 PC.

Prior to any experiments, both compartments were flushed with N_2 or O_2 for 30 min. During the electrolysis, a potential of −0.1 V was applied for 6 h. An aliquot of 100 µL was removed from both compartments before the experiments as well as after 1, 2, 4, and 6 h. Longtime experiments were performed in 8, 6 and 6 h increments on consecutive days.

The spectroscopic quantification of the H_2O_2 produced throughout the electrolysis experiments was performed according to a method published by Apaydin et al.,[90] and Su et al.[91] A solution of 4 mM *p*-nitrobenzeneboronic acid (Alfa Aesar) in dimethyl sulfoxide (DMSO) was combined in a 1:1 volumetric ratio with a 150 mM carbonate buffer,

prepared from Na_2CO_3 (Fluka) and $NaHCO_3$ (Sigma–Aldrich) at pH 9. The resulting mixture was filtered using a syringe filter (Chromafil RC-45/15 MS, Macherey-Nagel) and added to the analyte solution. After 36 min, during which the solution was stored in the dark, the UV–vis absorbance was measured at 411 nm using a Thermo Fischer Multiskan Go Microplate Spectrophotometer. The external calibration curve can be found in Figure S1 (Supporting Information), measured from several standard solutions of H_2O_2 (Merck).

Electrochemical impedance spectroscopy (EIS) was performed using an Ivium Vertex One.EIS potentiostat in a pH 7 phosphate buffer. The measurements were performed at the open circuit potential, which was determined for 300 s. The frequency was varied from 100 kHz to 100 mHz. Spectra were fitted using ZView software (Scribner Associated). The film thickness was determined using a Bruker DekTakXT stylus profilometer.

Characterization Methods: Infrared spectroscopy of the polymer-coated electrodes was performed using a Bruker VERTEX 80-ATR spectrometer in the spectral range of 4000–400 cm^{-1}, averaging 64 scans at a resolution of 4 cm^{-1}. Raman spectra were acquired using a Bruker MultiRAM at an excitation wavelength of 1064 nm in a spectral shift range between 3600 and 5 cm^{-1}. Morphology changes of the electrodes were monitored using a JEOL JSM-6360LV scanning electron microscope, operated under a high vacuum at an acceleration voltage of 7.0 kV. The contact angle measurements were performed on an Ossila Contact Angle Goniometer at room temperature using 18 mΩ of water. XPS measurements were performed on a Theta Probe XPS-system (Thermo Fisher), using a monochromated Al-Kα X-ray source with an energy of 1486.6 eV. The spot diameter on the sample surface was 400 µm. For high-resolution scans, the hemispherical analyzer was set to a pass energy of 20 eV at an energy step size of 0.05 eV. The system implements a dual flood gun, providing electrons and Ar^+ ions with low kinetic energy for charge compensation. Data acquisition and evaluation were performed via Avantage software (Thermo Fisher). For background correction, the smart background correction was used, based on a Shirley background modified by the constraint that the background values could not be at a higher intensity than the measured data. To correct charging, the binding energies of all spectra were referenced to the values of the typical C1s binding energy of aromatic C=C groups at 284.6 eV.[92]

Supporting Information

Supporting Information is available from the Wiley Online Library or from the author.

Acknowledgements

The authors thank the financial support of the Austrian Agency for International Cooperation in Education and Research (OeAD-GmbH, WTZ, CZ01/2020, 8J20AT025). D.W. acknowledges support from the Exzellenzstipendium des Bundesministeriums für Bildung, Wissenschaft und Forschung für Promovierte sub auspiciis Praesidentis. J.K. and J.R. thank project AKTION No. 95p3. Furthermore, the authors gratefully acknowledge financial support from the Austrian Science Foundation (FWF) within the Wittgenstein Prize for Prof. Sariciftci (Z222-N19). The open access publication of this work was supported by the Johannes Kepler Open Access Publishing Fund.

Conflict of Interest

D. W. has recently moved to work for the company EDL Anlagenbau.

Data Availability Statement

The data that support the findings of this study are available from the corresponding author upon reasonable request.

Keywords

anthraquinone derivatives, electropolymerization, heterogeneous electrocatalysis, oxygen reduction reaction, riboflavin

Received: August 7, 2023
Revised: December 11, 2023
Published online:

[1] K. Kalyanasundaram, M. Graetzel, *Curr. Opin. Biotechnol.* **2010**, *21*, 298.
[2] T. A. Faunce, W. Lubitz, A. W. (B). Rutherford, D. Macfarlane, G. F. Moore, P. Yang, D. G. Nocera, T. A. Moore, D. H. Gregory, S. Fukuzumi, K. B. Yoon, F. A. Armstrong, M. R. Wasielewski, S. Styring, *Energy Environ. Sci.* **2013**, *6*, 695.
[3] K. E. Dalle, J. Warnan, J. J. Leung, B. Reuillard, I. S. Karmel, E. Reisner, *Chem. Rev.* **2019**, *119*, 2752.
[4] M. Wang, H. Wang, H. Zhang, X. Li, *J. Energy Chem.* **2020**, *48*, 14.
[5] M. Chen, Q. Liu, Y. Zhang, G. Xing, S.-L. Chou, Y. Tang, *J. Mater. Chem. A* **2020**, *8*, 16061.
[6] S. Lee, J. Hong, K. Kang, *Adv. Energy Mater.* **2020**, *10*, 2001445.
[7] B. Häupler, A. Wild, U. S. Schubert, *Adv. Energy Mater.* **2015**, *5*, 1402034.
[8] D. Werner, D. H. Apaydin, E. Portenkirchner, *Batter. Supercaps* **2018**, *1*, 160.
[9] D. Werner, D. H. Apaydin, D. Wielend, K. Geistlinger, W. D. Saputri, U. J. Griesser, E. Drazevic, T. S. Hofer, E. Portenkirchner, *J. Phys. Chem. C* **2021**, *125*, 3745.
[10] J. M. Gallmetzer, S. Kröll, D. Werner, D. Wielend, M. Irimia-Vladu, E. Portenkirchner, N. S. Sariciftci, T. S. Hofer, *Phys. Chem. Chem. Phys.* **2022**, *24*, 16207.
[11] J. H. Montoya, L. C. Seitz, P. Chakthranont, A. Vojvodic, T. F. Jaramillo, J. K. Nørskov, *Nat. Mater.* **2017**, *16*, 70.
[12] D. G. Nocera, *Acc. Chem. Res.* **2017**, *50*, 616.
[13] F. Schüth, *Chem. Ing. Tech.* **2011**, *83*, 1984.
[14] N. S. Lewis, D. G. Nocera, *Proc. Natl. Acad. Sci. U S A.* **2007**, *104*, 15729.
[15] X. Huang, M. Song, J. Zhang, T. Shen, G. Luo, D. Wang, *Nano-Micro Lett.* **2023**, *15*, 86.
[16] S. Fukuzumi, Y. Yamada, *ChemElectroChem* **2016**, *3*, 1978.
[17] R. Ciriminna, L. Albanese, F. Meneguzzo, M. Pagliaro, *ChemSusChem* **2016**, *9*, 3374.
[18] J. M. Campos-Martin, G. Blanco-Brieva, J. L. G. Fierro, *Angew. Chem., Int. Ed.* **2006**, *45*, 6962.
[19] L. An, T. Zhao, X. Yan, X. Zhou, P. Tan, *Sci. Bull.* **2015**, *60*, 55.
[20] Y. Jiang, P. Ni, C. Chen, Y. Lu, P. Yang, B. Kong, A. Fisher, X. Wang, *Adv. Energy Mater.* **2018**, *8*, 1801909.
[21] J. S. Jirkovský, I. Panas, E. Ahlberg, M. Halasa, S. Romani, D. J. Schiffrin, *J. Am. Chem. Soc.* **2011**, *133*, 19432.
[22] Y. Lu, Y. Jiang, X. Gao, W. Chen, *Chem. Commun.* **2014**, *50*, 8464.
[23] Z. Zheng, Y. H. Ng, D.-W. Wang, R. Amal, *Adv. Mater.* **2016**, *28*, 9949.
[24] C. H. Choi, H. C. Kwon, S. Yook, H. Shin, H. Kim, M. Choi, *J. Phys. Chem. C* **2014**, *118*, 30063.
[25] P. S. Kauranen, E. Skou, *J. Electroanal. Chem.* **1996**, *408*, 189.
[26] Y. J. Sa, J. H. Kim, S. H. Joo, *Angew. Chem., Int. Ed.* **2019**, *58*, 1100.
[27] C. Zhu, He Li, S. Fu, D. Du, Y. Lin, *Chem. Soc. Rev.* **2016**, *45*, 517.
[28] V. Perazzolo, C. Durante, R. Pilot, A. Paduano, J. Zheng, G. A. Rizzi, A. Martucci, G. Granozzi, A. Gennaro, *Carbon* **2015**, *95*, 949.
[29] L. Li, C. Tang, Y. Zheng, B. Xia, X. Zhou, H. Xu, S.-Z. Qiao, *Adv. Energy Mater.* **2020**, *10*, 2000789.
[30] M. Vikkisk, I. Kruusenberg, U. Joost, E. Shulga, I. Kink, K. Tammeveski, *Appl. Catal. B* **2014**, *147*, 369.

[31] Y. Sun, I. Sinev, W. Ju, A. Bergmann, S. Dresp, S. Kühl, C. Spöri, H. Schmies, H. Wang, D. Bernsmeier, B. Paul, R. Schmack, R. Kraehnert, B. Roldan Cuenya, P. Strasser, *ACS Catal.* **2018**, *8*, 2844.
[32] T. Murata, K. Kotsuki, H. Murayama, R. Tsuji, Y. Morita, *Commun Chem.* **2019**, *2*, 46.
[33] M. Jakesová, D. H. Apaydin, M. Sytnyk, K. Oppelt, W. Heiss, N. S. Sariciftci, E. D. Glowacki, *Adv. Funct. Mater.* **2016**, *26*, 5248.
[34] H. Rabl, D. Wielend, S. Tekoglu, H. Seelajaroen, H. Neugebauer, N. Heitzmann, D. H. Apaydin, M. C. Scharber, N. S. Sariciftci, *ACS Appl. Energy Mater.* **2020**, *3*, 10611.
[35] V. G. Khomenko, V. Z. Barsukov, A. S. Katashinskii, *Electrochim. Acta* **2005**, *50*, 1675.
[36] R. P. Kingsborough, T. M. Swager, *Chem. Mater.* **2000**, *12*, 872.
[37] A. Rana, Y.-M. Lee, X. Li, R. Cao, S. Fukuzumi, W. Nam, *ACS Catal.* **2021**, *11*, 3073.
[38] B. Lv, X. Li, K. Guo, J. Ma, Y. Wang, H. Lei, F. Wang, X. Jin, Q. Zhang, W. Zhang, R. Long, Y. Xiong, U.-P. Apfel, R. Cao, *Angew. Chem., Int. Ed.* **2021**, *60*, 12742.
[39] J. Mason, C. Batchelor-Mcauley, R. G. Compton, *Phys. Chem. Chem. Phys.* **2013**, *15*, 8362.
[40] K. Tammeveski, K. Kontturi, R. J. Nichols, R. J. Potter, D. J. Schiffrin, *J. Electroanal. Chem.* **2001**, *515*, 101.
[41] A. Sehrish, R. Manzoor, K. Dong, Y. Jiang, Y. Lu, *Chem. Rep.* **2019**, *1*, 81.
[42] F. Mirkhalaf, K. Tammeveski, D. J. Schiffrin, *Phys. Chem. Chem. Phys.* **2004**, *6*, 1321.
[43] D. Wielend, M. Vera-Hidalgo, H. Seelajaroen, N. S. Sariciftci, E. M. Pérez, D. R. Whang, *ACS Appl. Mater. Interfaces* **2020**, *12*, 32615.
[44] A. Kerschbaumer, D. Wielend, E. Leeb, C. Schimanofsky, N. Kleinbruckner, H. Neugebauer, M. Irimia-Vladu, N. S. Sariciftci, *Catal. Sci. Technol.* **2023**, *13*, 834.
[45] T. Comeau Simpson, R. R. Durand, *Electrochim. Acta.* **1990**, *35*, 1399.
[46] D. L. DuBois, A. Miedaner, W. Bell, J. C. Smart, *Electrochemical and Electrocatalytic Reactions of Carbon Dioxide*, Elsevier B.V., Amsterdam **1993**.
[47] D. Wielend, D. H. Apaydin, N. S. Sariciftci, *J. Mater. Chem. A* **2018**, *6*, 15095.
[48] Z. Wang, J. Feng, X. Liu, H. Guo, *Atmosphere* **2022**, *13*, 543.
[49] C. Schimanofsky, D. Wielend, S. Kröll, S. Lerch, D. Werner, J. M. Gallmetzer, F. Mayr, H. Neugebauer, M. Irimia-Vladu, E. Portenkirchner, T. S. Hofer, N. S. Sariciftci, *J. Phys. Chem. C* **2022**, *126*, 14138.
[50] A. Kormányos, M. S. Hossain, G. Ghadimkhani, J. J. Johnson, C. Janáky, N. R. De Tacconi, F. W. Foss, Y. Paz, K. Rajeshwar, *Chem Eur. J.* **2016**, *22*, 9209.
[51] A. Kormányos, M. S. Hossain, F. W. Foss, C. Janáky, K. Rajeshwar, *Catal. Sci. Technol.* **2016**, *6*, 8441.
[52] L. Ivanová, J. Truksa, D. R. Whang, N. S. Sariciftci, C. Yumusak, J. Krajcovic, [Submitted] **2023**.
[53] J. Zhang, Q. Chi, E. Wang, S. Dong, *Electrochim. Acta* **1995**, *40*, 733.
[54] S. A Kumar, S.-M. Chen, *Sens Actuators, B* **2007**, *123*, 964.
[55] R. Sarma, M. J. Sloan, A. F. Miller, *ChemComm* **2016**, *52*, 8834.
[56] J. Richtar, P. Heinrichova, D. Apaydin, V. Schmiedova, C. Yumusak, A. Kovalenko, M. Weiter, N. Sariciftci, J. Krajcovic, *Molecules* **2018**, *23*, 2271.
[57] J. Richtar, L. Ivanova, D. R. Whang, C. Yumusak, D. Wielend, M. Weiter, M. C. Scharber, A. Kovalenko, N. S. Sariciftci, J. Krajcovic, *Molecules* **2021**, *26*, 27.
[58] A. Wang, A. Bonakdarpour, D. P. Wilkinson, E. Gyenge, *Electrochim. Acta* **2012**, *66*, 222.
[59] Q. Chi, S. Dong, *J. Electroanal. Chem.* **1994**, *369*, 169.
[60] E. Leeb, D. Wielend, C. Schimanofsky, N. S. Sariciftci, *Electrochem. Sci. Adv.* **2022**, *2*, e2100211.
[61] K. Wang, J. Huang, H. Chen, Y. Wang, S. Song, *ChemComm* **2020**, *56*, 12109.
[62] D. R. Whang, *Nano Convergence* **2020**, *7*, 37.
[63] K. Vaik, U. Mäeorg, F. C. Maschion, G. Maia, D. J. Schiffrin, K. Tammeveski, *Electrochim. Acta* **2005**, *50*, 5126.
[64] S. Zhang, Q. Fan, R. Xia, T. J. Meyer, *Acc. Chem. Res.* **2020**, *53*, 255.
[65] W. A. Badawy, K. M. Ismail, S. S. Medany, *Electrochim. Acta* **2006**, *51*, 6353.
[66] Y. Wei, Y. Sun, X. Tang, *J. Phys. Chem.* **1989**, *93*, 4878.
[67] T. Ohsaka, M. Ohba, M. Sato, N. Oyama, S. Tanaka, S. Nakamura, *J. Electroanal. Chem.* **1991**, *300*, 51.
[68] M. Gao, F. Yang, X. Wang, G. Zhang, L. Liu, *J. Phys. Chem. C* **2007**, *111*, 17268.
[69] K. M. Ismail, Z. M. Khalifa, M. A. Azzem, W. A. Badawy, *Electrochim. Acta.* **2002**, *47*, 1867.
[70] A. Radzevic, G. Niaura, I. Ignatjev, T. Rakickas, R. Celiesiute, R. Pauliukaite, *Electrochim. Acta* **2016**, *222*, 1818.
[71] X.-G. Li, Hu Li, M.-R. Huang, M. G. Moloney, *J. Phys. Chem. C* **2011**, *115*, 9486.
[72] Y. Ding, X. Ren, D. Chen, F. Wen, T. Li, F. Xu, *ACS Appl. Energy Mater.* **2022**, *5*, 3004.
[73] V. S. Jamadade, D. S. Dhawale, C. D. Lokhande, *Synth. Met.* **2010**, *160*, 955.
[74] W. Shao, R. Jamal, F. Xu, A. Ubul, T. Abdiryim, *Materials* **2012**, *5*, 1811.
[75] N. S. Sariciftci, H. Kuzmany, H. Neugebauer, A. Neckel, *J. Chem. Phys.* **1990**, *92*, 4530.
[76] M. Wagner, T. Rebis, O. Inganäs, *J. Power Sources* **2016**, *302*, 324.
[77] T. Sun, H. Du, S. Zheng, J. Shi, X. Yuan, L. Li, Z. Tao, *Small Methods* **2021**, *5*, 2100367.
[78] V. Ramakrishnan, N. Krishnamurthy, M. Gurunathan, V. J. P. Srivatsavoy, *Spectrochim. Acta, Part A* **1990**, *46*, 1615.
[79] J. Gasiorowski, A. I. Mardare, N. S. Sariciftci, A. W. Hassel, *Electrochim. Acta* **2013**, *113*, 834.
[80] A. Lodha, S. M Kilbey, P. C. Ramamurthy, R. V. Gregory, *J. Appl. Polym. Sci.* **2001**, *82*, 3602.
[81] Y. Kieffel, J. P. Travers, A. Ermolieff, D. Rouchon, *J. Appl. Polym. Sci.* **2002**, *86*, 395.
[82] R. C. Engstrom, V. A. Strasser, *Anal. Chem.* **1984**, *56*, 136.
[83] N. Wadnerkar, V. Gueskine, E. D. Glowacki, I. Zozoulenko, *J. Phys. Chem. A* **2020**, *124*, 9605.
[84] M. Warczak, M. Gryszel, M. Jakešová, V. Derek, E. D. Głowacki, *ChemComm* **2018**, *54*, 1960.
[85] D. Wielend, Y. Salinas, F. Mayr, M. Bechmann, C. Yumusak, H. Neugebauer, O. Brüggemann, N. S. Sariciftci, *ChemElectroChem* **2021**, *8*, 4360.
[86] P. Nunziante, G. Pistoia, *Electrochim. Acta* **1989**, *34*, 223.
[87] N. S. Sariciftci, M. Bartonek, H. Kuzmany, H. Neugebauer, A. Neckel, *Synth. Met.* **1989**, *29*, 193.
[88] D. Werner, C. Griesser, D. Stock, U. J. Griesser, J. Kunze-Liebhäuser, E. Portenkirchner, *ACS Appl. Energy Mater.* **2020**, *3*, 3477.
[89] Y. N. Ivanova, A. A. Karyakin, *Electrochem. Commun.* **2004**, *6*, 120.
[90] D. H. Apaydin, H. Seelajaroen, O. Pengsakul, P. Thamyongkit, N. S. Sariciftci, J. Kunze-Liebhäuser, E. Portenkirchner, *ChemCatChem* **2018**, *10*, 1793.
[91] G. Su, Y. Wei, M. Guo, *Am. J. Analyt. Chem.* **2011**, *2*, 879.
[92] G. C. Smith, *Updates in Applied Physics and Electrical Technology*, Springer Science and Business Media, New York **1994**.